Studies of Highly Excited Nuclear Bound Levels Using Neutron Capture Gamma Rays

B. ARAD (HUEBSCHMANN), G. BEN-DAVID (DAVIS), I. PELAH, AND Y. SCHLESINGER
Israel Atomic Energy Commission, Soreq Research Establishment, Rehovoth, Israel
(Received 27 August 1963)

Nuclear resonant scattering from individual levels has been observed using the discrete energy gamma rays produced by thermal neutron capture. This permits a study of the highly excited nuclear levels near the particle threshold region. It was found that only levels in nuclei in closed-shell regions have ground-state transition probabilities large enough to be detected by this method. An extension of the technique is suggested which permits variation of the gamma energy seen by the nucleus by about ±8 eV, using a rotating target.

I. INTRODUCTION

THE radiation widths of highly excited nuclear levels in the particle threshold energy region (6–10 MeV) have been studied mainly by three methods: neutron scattering, neutron capture, and nuclear elastic scattering of photons. The excited levels reached by neutron scattering and capture are virtual levels (unbound levels) and accurate measurements have been made only between the neutron binding energy and several tens of keV above this energy. On the other hand, the photon-scattering technique has been successfully applied in the energy region 5–20 MeV.

In the original work on nuclear elastic scattering, the photons were produced either as bremsstrahlung from betatron electrons,[1] or from charged-particle reactions, e.g., (p,γ).[2] In both these cases the gamma-ray spectra are essentially continuous, the energy resolution being several hundred keV for bremsstrahlung, and ~100 keV for (p,γ) reactions. Recently, a coincidence technique has been described[3] in which bremsstrahlung can be measured with an accuracy of up to 50 keV, but this technique has not yet been used extensively for resonant scattering studies. Hence, the above experiments gave scattering results averaged over energy intervals of between 100 keV and a few hundred keV.

These experiments show general agreement with the statistical model of the compound nucleus, especially if a Porter-Thomas distribution for radiation widths is assumed.[4]

However, there exist discrepancies between the cross sections obtained in the earlier "poor resolution" experiment,[1] and the moderate resolution experiment near 7 MeV.[2] These discrepancies have not yet been resolved even with a recent experiment having 1% resolution in the 6–11 MeV energy range.[5] An experiment having extremely high resolution would probably give more details of the fine structure of this resonance scattering.

It would, therefore, be desirable to use a source of essentially monoenergetic gamma rays for studying nuclear resonant scattering from individual levels. One such possible source is the capture gamma rays emitted from nuclei, following the absorption of thermal neutrons. These capture gamma rays have been extensively studied for the majority of elements,[6] and the energies measured to within several keV. The actual linewidth is much less than this, usually determined predominantly by the thermal Doppler broadening and of the order of a few eV at normal temperatures. These capture gamma rays, therefore, offer a suitable probe for examining the nature of the observed nuclear elastic scattering.

At first sight it would appear that the chance of an exact resonance condition between a capture gamma ray and a particular nuclear level is extremely small. However, examples of resonant scattering have recently been reported: the 7.285-MeV line of $Fe(n,\gamma)$ on lead,[7] the 5.44-MeV line of $Hg(n,\gamma)$ on Hg,[8] and nine additional resonances previously reported by the present authors.[9]

II. EXPERIMENTAL ARRANGEMENT

A. General Assembly

The general experimental arrangement is shown in horizontal section in Fig. 1. The gamma-ray source is inserted through a horizontal tube which penetrates the side access hole of the thermal column of the research reactor IRR-1 (this is a 5-MW pool-type reactor operated by the Israel Atomic Energy Commission). It is positioned some 60 cm from the side of the thermal column, so as to lie along the central axis

[1] E. G. Fuller and Evans Hayward, Phys. Rev. **101**, 692 (1956).
[2] K. Reibel and A. K. Mann, Phys. Rev. **118**, 701 (1960).
[3] J. S. O'Connel, P. A. Tipler, and P. Axel, Phys. Rev. **126**, 228 (1962).
[4] P. Axel, Phys. Rev. **126**, 671 (1962).
[5] P. Axel, K. Min, N. Stein, and D. C. Sutton, Phys. Rev. Letters **10**, 299 (1963).
[6] G. A. Bartholomew and L. A. Higgs, Atomic Energy Commission Laboratory Report AECL 669; L. V. Groshev, A. M. Demidov, V. N. Lutsenko, and V. I. Pelekhov, *Atlas of Gamma Ray Spectra from Radiative Capture of Thermal Neutrons* (Pergamon Press, New York, 1959).
[7] D. J. Donahue and C. S. Young, Atomic Energy Commission Report, TID-12093, p. 240 (unpublished). C. S. Young and D. J. Donahue, Bull. Am. Phys. Soc. **8**, 61 (1963). C. S. Young, thesis, The Pennsylvania State University, 1962 (unpublished).
[8] H. Fleishman, thesis, Technishe Hochschule, München, Germany, 1961 (unpublished).
[9] G. Ben-David and B. Huebschmann, Phys. Letters **3**, 82 (1962).

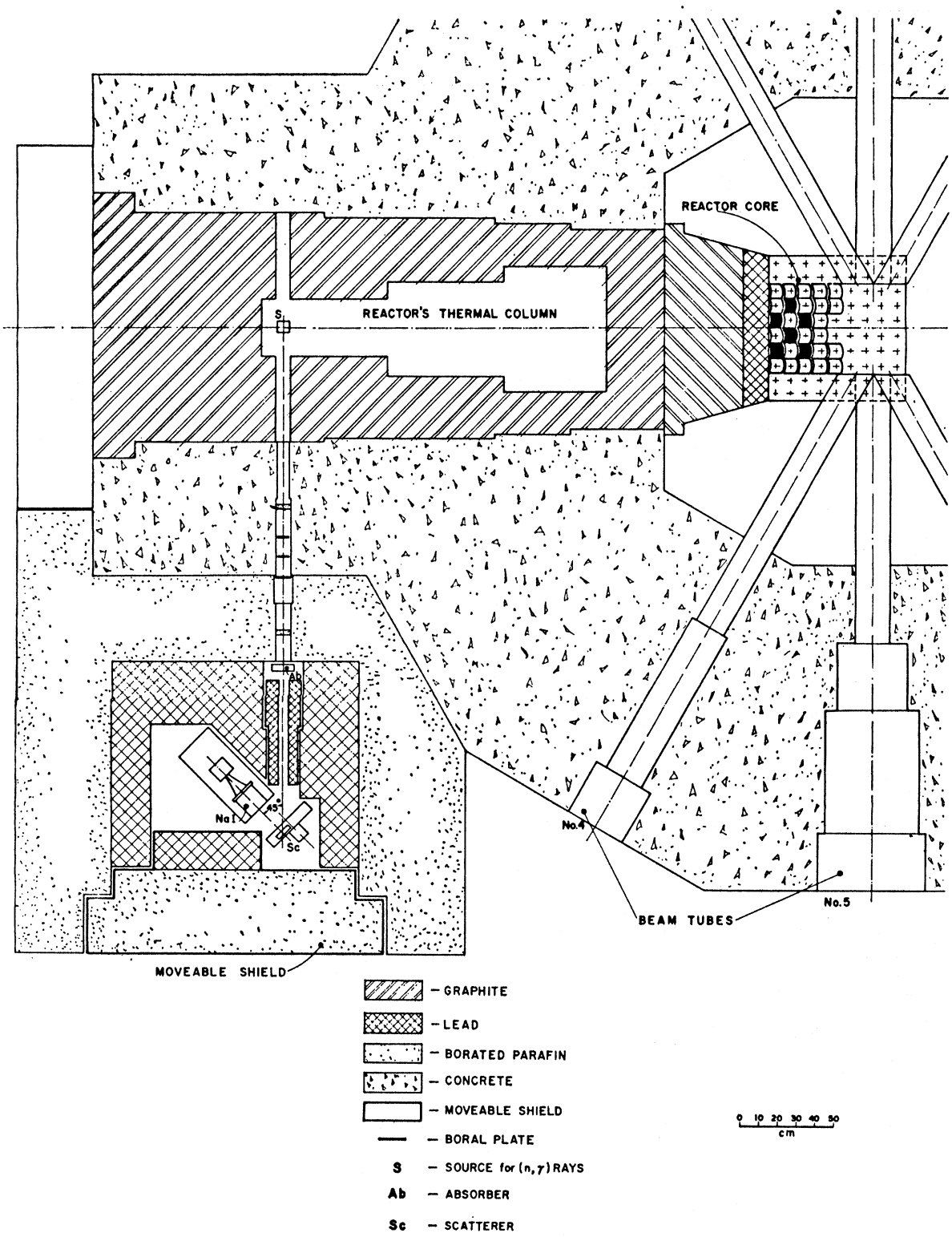

FIG. 1. Horizontal section of the experimental arrangement.

TABLE I. Details of the scattering targets.

Scatterer[a]	Chemical composition	Mass % of scatterer in target	Total thickness in mm	Total thickness in g/cm²	Actual thickness of scattering material (g/cm²)
Al	Metal	100	44.6	12.00	12.00
Bi	Metal	100	14.8	14.44	14.44
Ca	$CaCO_3$	40	38	2.03	0.81
Cr	Metallic powder	100	10	5.84	5.84
Cu	Metal	100	14.8	13.20	13.20
Dy	Dy_2O_3	87	10	2.36	2.05
Er	Er_2O_3	87.5	10	2.37	2.07
Fe	Metal	100	11.9	9.28	9.28
Gd	Gd_2O_3	87	10	2.38	2.07
Ho	Ho_2O_3	87.5	10	2.37	2.07
Hf	Metallic powder	100	8.5	2.41	2.41
Hg	$Hg_2(NO_3)_2 \cdot 2H_2O$	71.5	38	11.50	8.22
I	Crystalline	100	38	9.74	9.74
Mg	MgO_2	43	38	3.66	1.57
Mn	MnO_2	63	38	6.21	3.91
Na	$Na_2CO_3 \cdot H_2O$	37	38	4.34	1.61
Nd	Nd_2O_3	86	38	2.36	2.05
Ni	Metal	100	12.4	10.99	10.99
Pb	Metal	100	14.8	15.84	15.84
Pb^{206}	$PbCO_3$	78	38	8.48	6.6
Pr	Pr_2O_3	85.5	15	2.36	2.02
S	Powder	100	38	2.31	2.31
Sm	Sm_2O_3	86	10	2.40	2.06
Sn	Metal	100	14.8	10.84	10.84
Y	Y_2O_3	78.5	10	2.37	1.86
Yb	Yb_2O_3	88	8.5	2.34	2.06

[a] All of these samples, with the exception of Pb^{206}, were of natural isotopic abundance.

at maximum flux position. The resulting gamma-ray beam passes back through the horizontal tube and a hole in the side shielding of the thermal column. The beam is then collimated with a 55-cm-thick lead collimator having an aperture of 52 mm. The scattering sample is placed at the center of this collimated beam, at a distance of 250 cm from the gamma source.

Because of the low counting rate in the detector during scattering measurements, it was essential to reduce the background due to reactor operation and cosmic radiation. The scatterer and detector were surrounded with lead, 55 cm thick in the direction of the reactor shielding walls, and 20 cm thick in all other directions. The lead shield itself was surrounded by a 45-cm-thick borated paraffin layer to remove stray neutrons entering from the reactor. In addition, the horizontal access tube was shielded with several layers of boron and paraffin to remove neutrons scattered into the beam direction. It was found that stray neutrons produced background (n,γ) reactions in the vicinity of the detector, and the paraffin shield permitted a background reduction of a factor of 30 in the 6–9 MeV energy range. A section of the shielding was mounted on a trolley, permitting access to the detector and scatterer and manual adjustments of the respective angles relative to the incident gamma beam.

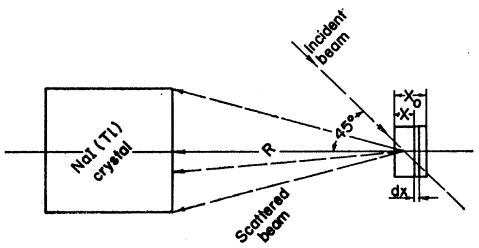

FIG. 2. Scattering geometry.

B. Detector and Beam Monitor

The detector used in the present experiment was a Harshaw matched window 5-in.-diam×5-in.-thick NaI(Tl) crystal mounted on a 3-in.-diam 6363 photomultiplier. The crystal was fitted on a graduated rotating arm, the center of rotation positioned on the central axis of the gamma-ray beam, together with the scattering target. In the normal scattering position the detector made an angle of 135° with the incident gamma-ray beam, the scattering target lying parallel to the crystal face, as seen from Fig. 2. In order to measure the incident gamma-ray beam the detector was rotated to the 0° position in line with the beam. However, at full reactor power, the direct gamma intensity was several orders of magnitude too high for the detector, causing overloading of the electronic equipment. Hence, for the incident beam measurements either the power level of the reactor was reduced, or, alternatively, an additional collimator of 5-mm aperture was inserted inside the main collimator, effectively attenuating the gamma beam by a factor of about 100.

The direct and scattered spectra were recorded with

TABLE II. Capture gamma-ray sources and their properties.[a]

Source	Chemical composition	Mass kg	Principal γ rays (in MeV)
Al	Metal	1.640	7.73
Cl	polyvinyl Chloride	0.380	8.55, 7.78, 7.41, 6.96, 6.64, 6.12, 5.72
Co	CoO	0.230	7.49, 7.20, 6.98, 6.87, 6.68, 6.48, 5.97, 5.67
Cr	Metallic powder	0.480	9.72, 8.88, 8.49, 7.93, 7.09, 6.65, 5.60
Cu	Metal	1.860	7.91, 7.63, 7.29, 7.14, 7.00, 6.63
Fe	Metallic powder	0.440	9.30, 7.64, 7.28, 6.03
Hg	$Hg_2(NO_3)_2 \cdot 2H_2O$	0.310	6.44, 6.31, 5.99, 5.67, 5.44
Mn	MnO_2	0.240	7.26, 7.15, 7.04, 6.96, 6.79, 6.10, 5.76
Ni	Metal	0.900	9.00, 8.50, 8.10, 7.83, 7.58, 6.84, 6.64
Ti	TiO_2	0.210	6.75, 6.56, 6.42
V	V_2O_5	0.120	7.30, 7.16, 6.86, 6.51, 6.46, 5.87, 5.73
Y	Y_2O_3	0.200	6.07, 5.63

[a] For more detailed information, additional lines, intensities, etc., see Ref. 6.

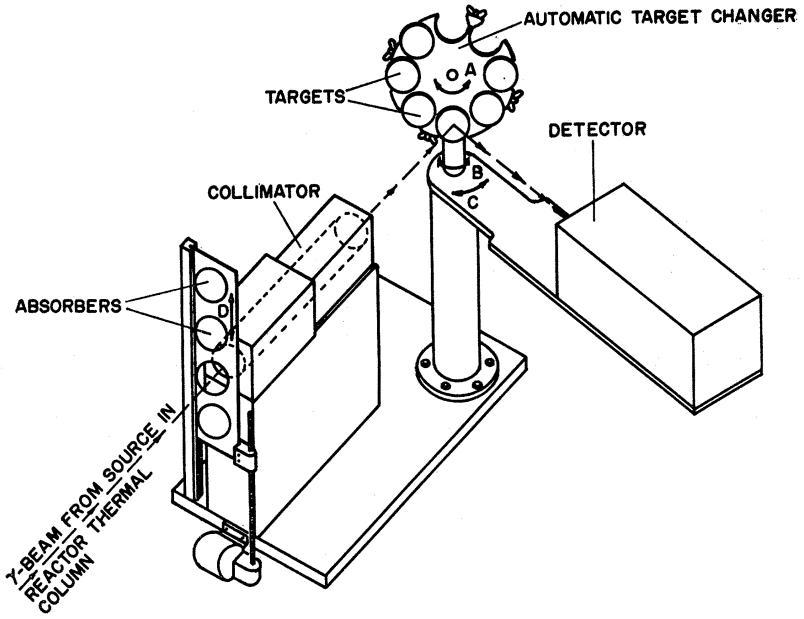

FIG. 3. Schematic diagram of the experimental setup.

a transistorized pulse-height analyzer, using either a 400-channel Intertechnique or a 512-channel Radiation Counter Laboratories. The over-all stability was usually better than ± 2 channels per day, corresponding to some 100 keV. However, it was possible to measure the peak energy of the scattered gamma rays to within 50 keV, which was usually sufficient to permit unambiguous identification of the particular gamma line responsible for the resonant scattering.

During long runs it was necessary to monitor the intensity of the incident gamma-ray beam independently of the reactor power level instruments. Owing to local flux changes induced by control rods or reactor poisons, there is no direct proportionality between the neutron flux in the thermal column and the flux recorded by the reactor instruments. Over a period of a few days this nonproportionality can introduce an error of up to 15%. It was, therefore, necessary to monitor the flux inside the thermal column itself. A lithium coated surface barrier solid-state counter was inserted into the thermal column[10] near the source position, and the resultant pulses due to either alphas or tritons were monitored automatically. It was found experimentally that the gamma-ray beam intensity was proportional to this monitored neutron flux to within 1%.

C. Scattering Arrangement and Geometry

Properties of the scatterers used are given in Table I. The powder samples were enclosed in perspex containers whose wall thickness did not exceed 0.2 g/cm^2. During the general scattering measurements, the samples were mounted on a disk holding eight scatterers, as seen in Fig. 3. The disk could be rotated about a horizontal axis, bringing consecutively each scatterer

[10] B. Huebschmann and S. Alterowitz, Res. Reactor J. 3, 11 (1963).

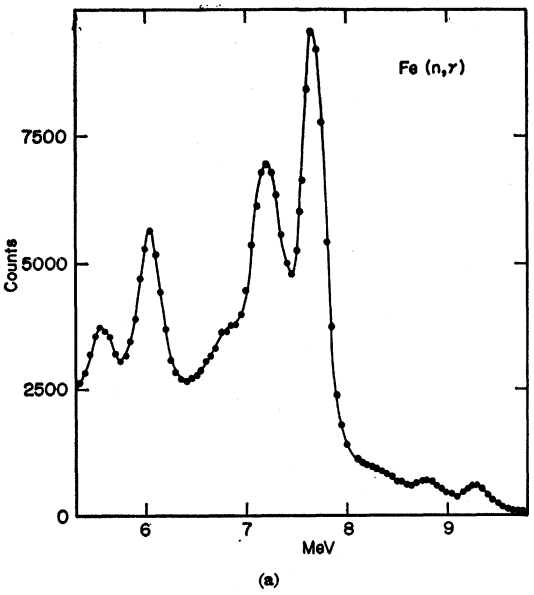

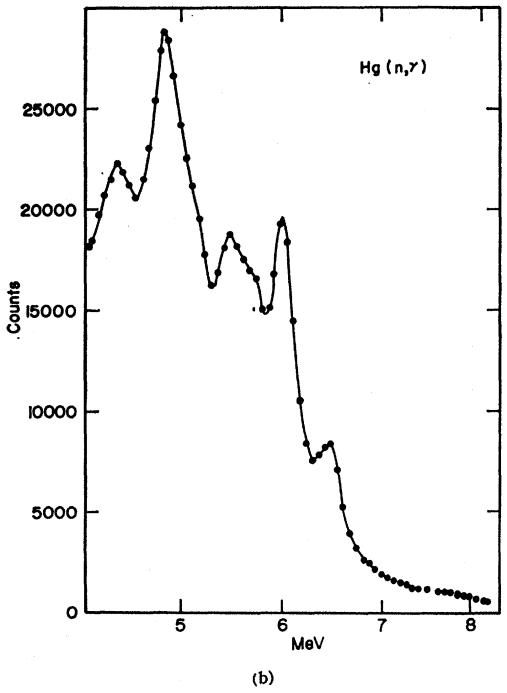

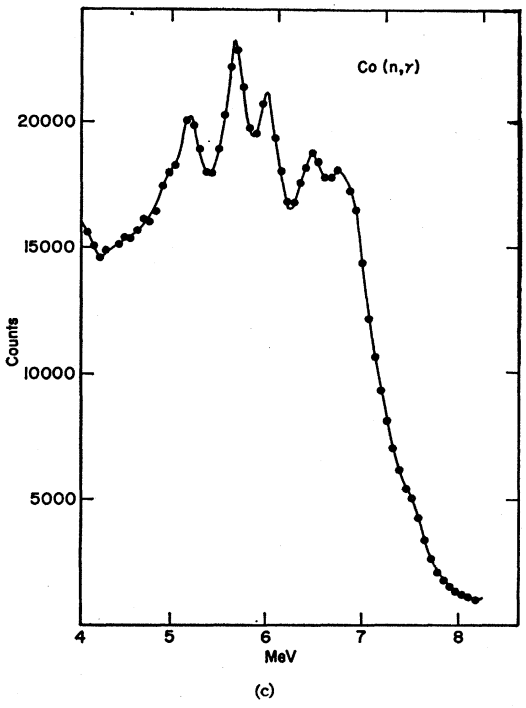

FIG. 4. A few examples of direct spectra from capture gamma-ray sources, using a 5-mm collimated beam and a 5-in.-diam, 5-in.-thick NaI(Tl) crystal. Recording time two minutes at 1.5-MW reactor power. (a) The (n,γ) spectrum of iron; (b) the (n,γ) spectrum of mercury; (c) the (n,γ) spectrum of cobalt.

into the direct gamma beam. This permitted automatic operation; eight samples were measured before the disk had to be reloaded.

The scattering disk could also be rotated around a vertical axis and, hence, the scattering angle adjusted as required. In the usual setting the angle between the gamma-ray beam and the scatterer was 45°.

D. Gamma-Ray Sources

The gamma-ray sources were irradiated in the thermal column at a thermal flux of about 10^{10} neutron/$cm^2 \cdot sec$, for a reactor power level of 1.5 MW. In order to achieve this flux at the source position it was necessary to remove a large proportion of the graphite between the source and the reactor core. This permitted an increase in flux of a factor of approximately 100, with a slight reduction in the cadmium ratio.

Details of the sources are given in Table II. The direct spectra were recorded with the crystal rotated in line with the gamma beam, using a 0.5-cm-diam collimator, and are shown in Fig. 4.

E. General Scattering Measurements

A general survey was carried out using all the possible combinations of scatterers and sources to look for nuclear scattering resonances. For this survey the scatterer was placed at an angle of 45° to the gamma beam, and the detector at an angle of 135°. Collectively, some 20 clear examples of resonance effects have been observed so far, including the events previously

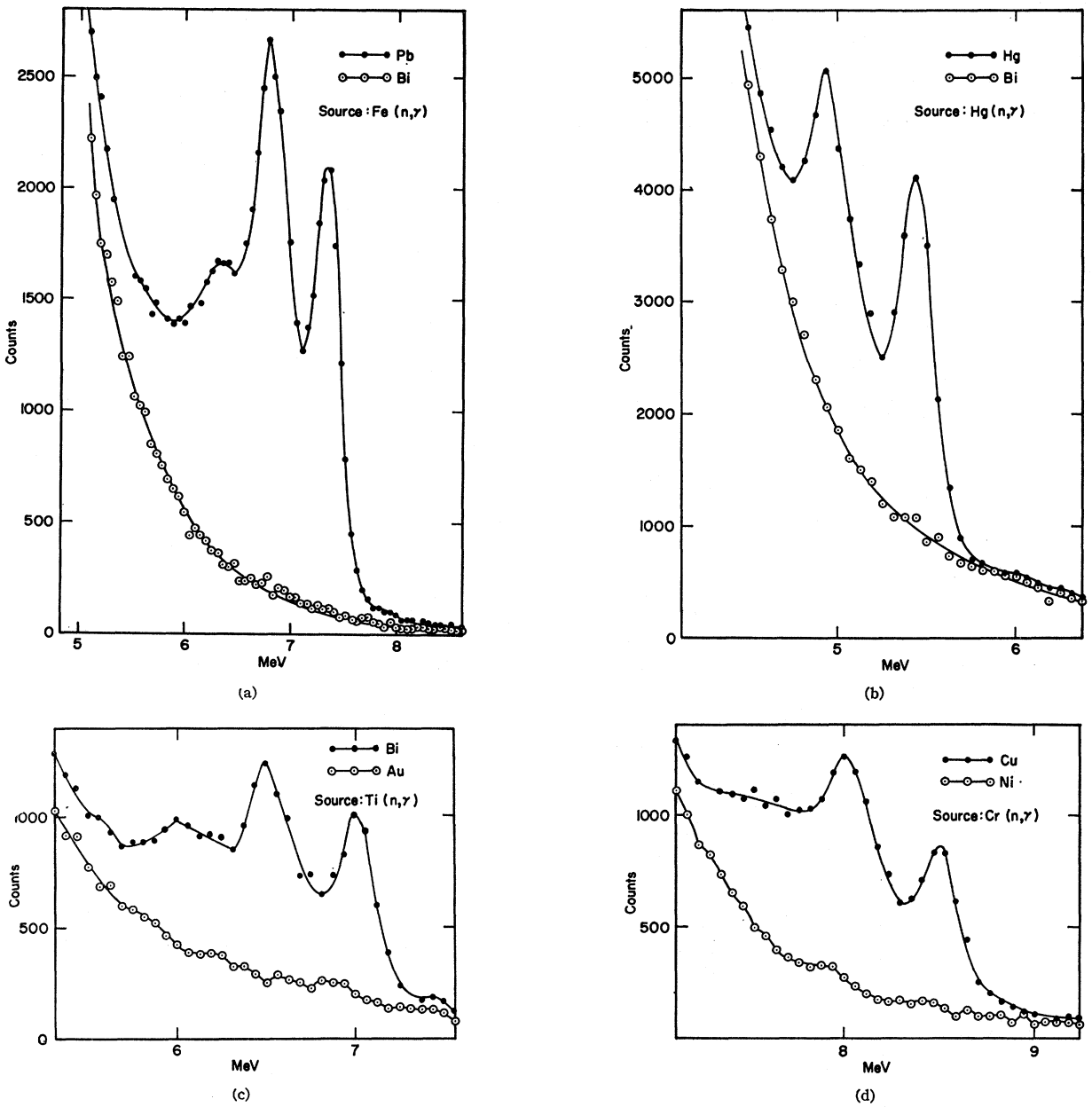

FIG. 5. A few representative spectra of resonant scattered gamma rays. Recording time 2 h at 1.5-MW reactor power. (a) The resonant scattered spectrum from lead (7.285 MeV) compared with nonresonant scattered spectrum from bismuth. (b) The resonant scattered spectrum from mercury (5.44 MeV) compared with nonresonant scattered spectrum from bismuth. (c) The resonant scattered spectrum from bismuth (6.996 MeV) compared with nonresonant scattered spectrum from gold. (d) The resonant scattered spectrum from copper (8.499 MeV) compared with nonresonant scattered spectrum from nickel. (e) The resonant scattered spectrum from samarium (8.997 MeV) compared with nonresonant scattered spectrum from cerium. (f) The resonant scattered spectrum from neodymium (6.887 MeV) compared with nonresonant scattered spectrum from samarium. (g) The resonant scattered spectrum from lead (7.38 MeV) compared with nonresonant scattered spectrum from bismuth. (h) The resonant scattered spectrum from lead (7.305 MeV) compared with nonresonant scattered spectrum from bismuth. (i) The resonant scattered spectrum from lead (6.98 MeV) compared with nonresonant scattered spectrum from bismuth. (j) The resonant scattered spectrum from nickel (7.639 MeV) compared with nonresonant scattered spectrum from copper. (k) Spectrum of resonant scattered gamma rays from lead (6.98 MeV). The curve represents the difference between the resonant scattering and the nonresonant background from bismuth. Standard errors are shown in the diagram.

FIG. 5. (*continued*).

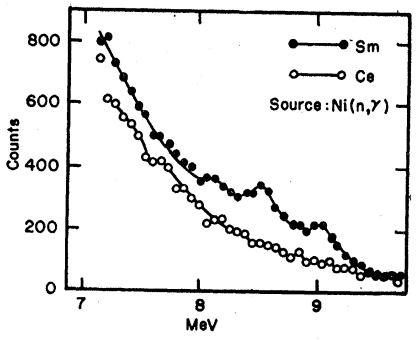

(e)

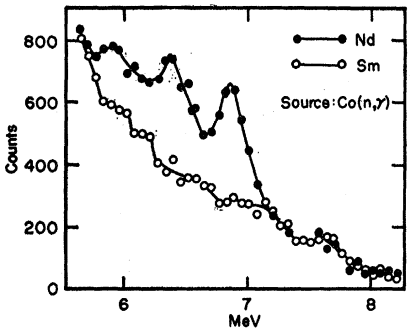

(f)

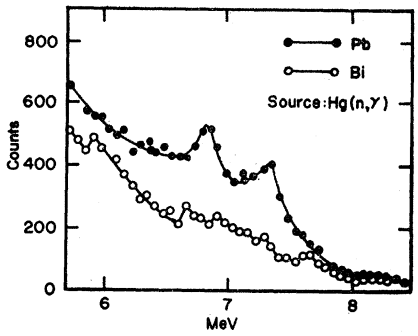

(g)

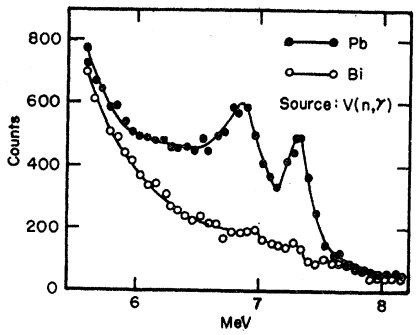

(h)

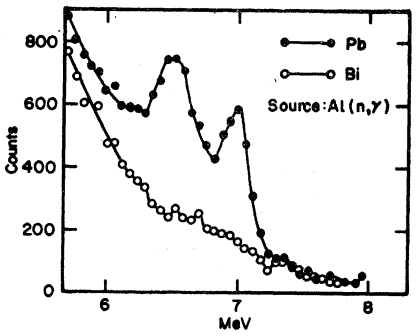

(i)

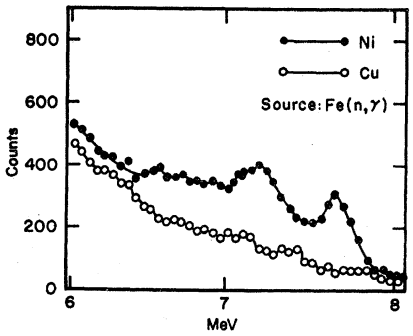

(j)

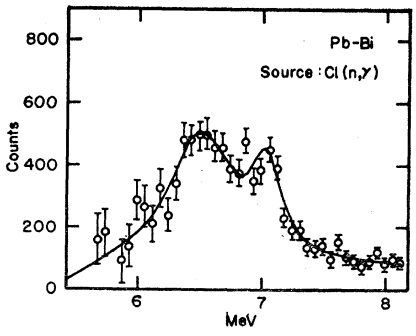

(k)

reported,[7–9] and these are shown in Fig. 5 together with spectra produced by nonresonant scattering in targets of comparable thickness and charge.

F. Temperature Variation Measurements

It is of interest to measure the intensity variation of the resonantly scattered radiation as a function of the scatterer temperature, as this furnishes additional information on the level widths responsible for the resonance.

For low temperatures a styrofoam container was used, the scatterer being in direct contact with liquid nitrogen. The γ beam had only to penetrate a 4-cm layer of Styrofoam (0.1 g/cm^2) before reaching the scatterer.

For temperatures above room temperature, an electrical oven was used, permitting temperature variation of the scatterer up to 650°C. The temperature could be preadjusted and, using a thermostatic

control unit, automatically held constant to within a few degrees.

G. Energy Variation of the Neutron Capture Gamma Rays

Further information on the resonances reported in this work could be obtained by changing the gamma-ray energy by a few electron volts. This would permit an increase or decrease in the separation between the gamma line and the peak resonance energy and, in favorable cases, a direct measurement of the separation δ for gammas from thermal neutron capture. Two methods suggest themselves for altering the energy of the capture gamma rays. The first is to use capture gamma rays produced by epithermal neutrons, the resulting recoil energy producing a corresponding energy change in the photons. A time-of-flight technique can be used to select the neutron energies. The second method is to use capture gamma rays from thermal neutron capture, and to rapidly rotate the scattering target, thus causing a Doppler shift in the photon energy seen by the nucleus.

These two methods have been compared[11] and it was shown that the rotating target technique has a counting rate at least two orders of magnitude higher than the time-of-flight technique and, in addition, the advantage of obtaining an equal shift in either positive or negative direction.

A rotating target is being prepared in this laboratory, using a scattering ring of 20-cm radius, and a maximum of 15 000 rpm. This corresponds to a maximum velocity of 300 m/sec. The resulting Doppler energy shift equals $\pm 10^{-6}E_0$, giving ± 8 eV for an energy E_0 of 8 MeV.

III. ANALYSIS OF THE DATA

A. Scattered Intensity Reaching Detector

The over-all efficiency for detection of the elastically scattered photons is modified by electronic and nuclear absorption in the scattering target. Consider a collimated beam of $F(E)dE$ photons per second in the energy interval $E-E+dE$, striking the target at an incident angle of 45° (Fig. 2). The number of photons scattered by a layer of thickness dx cm at depth x cm in the target and reaching the detector at an average scattering angle of 135° is given by

$$S(E,x)dxdE=F(E)\frac{\sigma_{\gamma\gamma}\Delta\Omega N}{11.2}\times\exp\left\{-\left[\frac{(\sigma_n+\sigma_e)}{\cos 45^\circ}+\sigma_e\right]Nx\right\}dxdE, \quad (1)$$

where $\sigma_{\gamma\gamma}$ is the cross section for nuclear resonant scattering, $\Delta\Omega$ the average solid angle subtended by the detector for scattered photons, N the number of target nuclei per unit volume, σ_n the total nuclear cross section, and σ_e the total electronic cross section, including absorption and scattering. The factor 11.2 expresses the ratio between the integral cross section $\sigma_{\gamma\gamma}$ and the differential cross section per unit solid angle at an angle of 135° for an assumed dipole distribution $(1+\cos^2\vartheta)$. It should be noted that all these cross sections are energy-dependent, although σ_e does not vary over the width of a capture gamma ray (a few eV).

In deriving the above formula it is assumed that after a resonance scatter, the recoil energy loss is sufficient to remove the photon from the resonance condition with the nuclear level causing the resonance. For a photon of 7 MeV, and target nuclei of mass 150, this recoil energy amounts to ~170 eV.

By integrating over the target thickness, the number of photons in the energy range $E-E+dE$ reaching the detector can be derived as

$$S(E)dE=\int_0^{x_0}S(E,x)dEdx=\frac{F(E)\sigma_{\gamma\gamma}\Delta\Omega}{11.2[\sqrt{2}\sigma_n+(1+\sqrt{2})\sigma_e]}\times[1-\exp\{-[\sqrt{2}\sigma_n+(1+\sqrt{2})\sigma_e]Nx_0\}]dE. \quad (2)$$

The total intensity I_{sc} of scattered radiation is obtained by integrating $S(E)dE$ over the energy range of interest, in this case the capture gamma-ray energy region described by $F(E)$. The appropriate procedure for integrating Eq. (2) depends on the ratio of the quantities σ_n and σ_e in this energy region.

1. $\sigma_n \ll \sigma_e$

In this case, the terms involving σ_n can be neglected, and taking σ_e as constant over the region of integration one obtains

$$I_{sc}=\frac{\Delta\Omega}{11.2}\frac{1-\exp[-(1+\sqrt{2})\sigma_e Nx_0]}{(1+\sqrt{2})\sigma_e}\times\int_0^\infty\sigma_{\gamma\gamma}(E)F(E)dE. \quad (3a)$$

2. $\sigma_n \gtrsim \sigma_e$

A convenient solution can be obtained only for relatively thin scatterers, permitting the expansion of the exponential term to the first and second order, giving

$$I_{sc}=\frac{\Delta\Omega}{11.2}Nx_0\times\left[\left(1-\frac{Nx_0(1+\sqrt{2})\sigma_e}{2}\right)\int_0^\infty\sigma_{\gamma\gamma}(E)F(E)dE-\frac{Nx_0}{\sqrt{2}}\int_0^\infty\sigma_{\gamma\gamma}(E)F(E)\sigma_n(E)dE\right], \quad (3b)$$

[11] G. Ben-David, B. Heubschmann, and I. Pelah, Israel Atomics-842 (unpublished); Nucl. Instr. & Methods (to be published).

where terms above the second order are neglected.

It is convenient to define an effective cross section $\langle\sigma_{\gamma\gamma}\rangle$ by

$$\langle\sigma_{\gamma\gamma}\rangle=\int_0^\infty \sigma_{\gamma\gamma}F(E)dE \Big/ \int_0^\infty F(E)dE. \quad (4)$$

Substituting in Eqs. (3a) and (3b) we obtain

$$I_{sc}=\frac{\Delta\Omega}{11.2}\frac{1-\exp[(1+\sqrt{2})\sigma_e N x_0]}{(1+\sqrt{2})\sigma_e}\langle\sigma_{\gamma\gamma}\rangle\int_0^\infty F(E)dE, \quad (5a)$$

$$I_{sc}=\frac{\Delta\Omega}{11.2}Nx_0 \times\left[1-\frac{Nx_0(1+\sqrt{2})\sigma_e}{2}\right]\langle\sigma_{\gamma\gamma}\rangle\int_0^\infty F(E)dE - \frac{\Delta\Omega}{11.2}\frac{N^2x_0^2}{\sqrt{2}}\int_0^\infty \sigma_{\gamma\gamma}F(E)\sigma_n dE. \quad (5b)$$

In practice, the second term of Eq. (5b) contributed, at most, a few percent and could usually be neglected.

B. Evaluation of $\langle\sigma_{\gamma\gamma}\rangle$ from the Experimental Results

In Fig. 5 typical spectra of resonantly scattered photons are shown. It is convenient to measure the area under the photopeak rather than the total area, in determining the cross section. The counting rate under the photopeak is given by

$$C_{sc}=\epsilon\eta_{sc}I_{sc}, \quad (6)$$

where ϵ is the detector efficiency and η_{sc} the photofraction for the scattered radiation. C_{sc} is corrected for the nonresonant background.

A derivation of $\Delta\Omega$ has been given in the literature.[1]

$$\Delta\Omega=A/R^2\int_0^L\frac{e^{-\mu t}}{(R+t)^2}dt \Big/ \int_0^L\frac{e^{-\mu t}}{R^2}dt,$$

where L is the length of the crystal, A its cross-sectional area, μ the linear absorption coefficient for sodium iodide, and R the distance from the center of the target to the center of the front face of the crystal.

For the 5-in. height of crystal used in this work and a distance $R=17$ cm, the integrals can be evaluated to give $\Delta\Omega=0.29$.

The evaluation of $\langle\sigma_{\gamma\gamma}\rangle$ from Eqs. (5) and (6) requires the determination of $\int_0^\infty F(E)dE$. The direct spectrum was measured with the detector in the 0° position, the counting rate under the photopeak being given by

$$C_0=\epsilon\eta_0\int_0^\infty F(E)dE, \quad (7)$$

where η_0 is the photofraction for a collimated beam parallel to the axis. Equations (5), (6), and (7) permit a solution of $\langle\sigma_{\gamma\gamma}\rangle$

$$\langle\sigma_{\gamma\gamma}\rangle=\frac{C_{sc}}{C_0}\frac{\eta_0}{\eta_{sc}}\frac{11.2}{\Delta\Omega}\frac{(1+\sqrt{2})\sigma_e}{1-\exp[-(1+\sqrt{2})\sigma_e N x_0]}, \quad (8a)$$

or for a thin scatterer

$$\langle\sigma_{\gamma\gamma}\rangle=\frac{C_{sc}}{C_0}\frac{\eta_0}{\eta_{sc}}\frac{11.2}{\Delta\Omega}\frac{1}{Nx_0}\frac{2}{2-Nx_0\sigma_e(1+\sqrt{2})}, \quad (8b)$$

neglecting the last term in (5b).

C. Evaluation of the Level Width and Separation δ between the Photon Line and the Resonance Level

The effective cross section $\langle\sigma_{\gamma\gamma}\rangle$ for nuclear resonant scattering is found by integrating over energy the product of the gamma-line spectrum $F(E)$ and the nuclear elastic scattering cross section $\sigma_{\gamma\gamma}(E)$, as shown in Eq. (4).

The elastic scattering cross section of an isolated level for photons of energy E is given by[12]

$$\sigma_{\gamma\gamma}(E,t_i)=\sigma_{\max}{}^0\Psi(x,t_i), \quad (9)$$

where

$$\sigma_{\max}{}^0=2\pi\lambda\!\!\!^{-2}g\left(\frac{\Gamma_0}{\Gamma}\right)^2, \quad (10)$$

$\lambda\!\!\!^{-}$ being the photon wavelength divided by 2π; g the spin factor [$g=(2j_e+1)/(2j_g+1)$, j_e, j_g the spins of excited and ground states]; Γ_0 is the level width for the ground-state transition; and Γ is the total width.

The function Ψ takes into account Doppler broadening caused by thermal motion of the scattering nuclei and is defined by

$$\Psi(x,t_i)=\frac{1}{2(\pi t_i)^{1/2}}\int_{-\infty}^{+\infty}\frac{e^{-(x-y)^2/4t_i}}{1+y^2}dy, \quad (11)$$

where $x=2(E-E_R)/\Gamma$, E_R being the peak resonance energy. $t_i=(\Delta_i/\Gamma)^2$, where Δ_i is the Doppler width defined by

$$\Delta_i=E_R(2kT_i/M_0c^2)^{1/2}, \quad (12)$$

with k the Boltzmann constant, T_i the effective temperature,[13] M_0 the mass of the scattering nucleus, and c the velocity of light.

At normal temperatures and for energies about 8 MeV above the ground state, the Doppler width Δ_i lies in the 4–8 eV range.

Tables of Ψ appear in the literature.[14] For values of $t_i\gg1$ and distances from the peak energy $|E-E_R|$

[12] F. R. Metzger, Progr. Nucl. Phys. **7**, 53 (1959).
[13] W. E. Lamb, Phys. Rev. **55**, 190 (1939).
[14] M. E. Rose, W. Miranker, P. Leak, L. Rosenthal, and J. K. Hendrickson, Westinghouse Electric Corporation Atomic Power Div. Report WAPD-SR-506, 1954, Vols. I and II (unpublished).

$\ll\Delta_i^2/\Gamma$, Eq. (11) can be expressed in the pure Doppler form

$$\Psi(x,t_i)=(\pi)^{1/2}\frac{\Gamma}{2\Delta_i}\exp\left[-\frac{(E_R-E)^2}{\Delta_i^2}\right]. \quad (13)$$

Similarly a gamma line having natural width Γ_e can be shown to have a Doppler-broadened shape given by

$$F(E)dE=C\Psi(x_e,t_e)dE, \quad (14)$$

where C is an arbitrary constant. The function $\Psi(x_e,t_e)$ is defined in a similar form to Eq. (11) by

$$\Psi(x_e,t_e)=\frac{1}{2(\pi t_e)^{1/2}}\int_{-\infty}^{+\infty}\frac{\exp[-(x_e-z)^2/4t_e]}{1+z^2}dz, \quad (15)$$

with $x_e=2(E_e-E)/\Gamma_e-E_e$ the peak energy of the gamma line (having corrected for recoil in the emitting nucleus); $t_e=(\Delta_e/\Gamma_e)^2-\Delta_e$ the Doppler width of the emitting nucleus.

Inserting the expressions for $F(E)$ and $\sigma_{\gamma\gamma}(E)$, (9) and (14) in Eq. (4), we find

$$\langle\sigma_{\gamma\gamma}\rangle=\sigma_{\max}{}^0\int_0^\infty\Psi(x_e,t_e)\Psi(x,t_i)dE\Big/\int_0^\infty\Psi(x_e,t_e)dE. \quad (16)$$

This integration over a product of two Ψ functions has been solved[15] giving

$$\langle\sigma_{\gamma\gamma}\rangle=\frac{\sigma_{\max}{}^0}{1+\beta}\Psi(x_1,t_1) \quad (17)$$

with

$$x_1=2|E_R-E_e|/(\Gamma_e+\Gamma),$$
$$t_1=(\Delta_e^2+\Delta_i^2)/(\Gamma_e+\Gamma)^2, \quad (18)$$
$$\beta=\Gamma_e/\Gamma.$$

In evaluating the energy difference term $\delta=|E_R-E_e|$ between the peak photon line and resonance level, the recoil energy term $E_e^2/2M_0c^2$ must be subtracted from E_e. This can total several hundred eV for photons of 8 MeV.

The use of Eq. (17) involves a knowledge of the ratio β between the linewidths Γ_e and Γ. However, if the gamma line has the pure Doppler form of (13), Eq. (17) can be expressed in the form

$$\langle\sigma_{\gamma\gamma}\rangle=\sigma_{\max}{}^0\Psi(x_2,t_2), \quad (19)$$

where

$$x_2=2|E_R-E_e|/\Gamma,$$
$$t_2=(\Delta_e^2+\Delta_i^2)/\Gamma^2. \quad (20)$$

Hence Eq. (19) involves only Γ, and $\delta=|E_R-E_e|$ as unknown parameters Δ_R, Δ_i are calculable if the ambient temperature and Debye temperatures are known.[13]

However, the use of Eq. (19) implies the pure Doppler form for the incident radiation. Consider thermal neutron capture gamma rays. If the photons are emitted in a ground-state transition, the original linewidth is given entirely by the Maxwellian energy spread of the thermal neutrons, and Eq. (19) is exact in this case. Even where the capture gamma ray is emitted in transition to a low-lying state, the natural linewidth is likely to be less than 10 meV,[16] again permitting the use of (19) for δ many times the Doppler width Δ_e.

By changing the scatterer temperature, information can be obtained on both the width of the resonance level and the separation δ. Consider two temperatures, T_i, T_j of the scatterer. The ratio of counting rates is given by

$$C_{sc}(i)/C_{sc}(j)=\Psi(x_2,t_{2i})/\Psi(x_2,t_{2j}) \quad (21)$$

with

$$t_{2i}=(\Delta_e^2+\Delta_i^2)/\Gamma^2,$$
$$t_{2j}=(\Delta_e^2+\Delta_j^2)/\Gamma^2.$$

By plotting the experimental ratios $C_{sc}(i)/C_{sc}(j)$ and using Eq. (19), a relation between the quantities Γ, Γ_0, and δ can be derived. Under favorable conditions, the temperature variation can give a unique solution for δ and Γ_0^2/Γ. Figure 6 shows the expected ratios of counting rates as functions of temperature for different values of the parameters δ and Γ for a particular case.

D. Self-Absorption Experiment

In the preceding section a method was described for evaluating the separation between the photon and resonance lines, and obtaining a relation between Γ_0 and Γ, the partial and total level widths. A different experiment must be performed if the level widths are to be evaluated separately. In favorable cases where $\sigma_n\sim\sigma_e$ it is possible to carry out a self-absorption experiment by inserting a target of the scattering material in the incident beam before the main scattering target.

The intensity of radiation reaching the detector is now modified by both nuclear and electronic absorption in the additional target. In practice, two absorbers are used, the resonant absorber, and a nonresonant absorber having nuclear charge adjacent to that of the resonant nucleus. The two absorbers thicknesses are chosen to as to have equal electronic absorption.

We now define an experimental ratio R by

$$R=\frac{\text{Scattering intensity with nonresonant absorber}-\text{scattering intensity with resonant absorber}}{\text{Scattering intensity with nonresonant absorber}}. \quad (22)$$

[15] B. Arad, G. Ben-David, and Y. Schlessinger, Nucl. Phys. (to be published).
[16] S. Devons, in *Nuclear Spectroscopy*, edited by Fay Ajzenberg-Selove (Academic Press Inc., New York, 1960), Chap. IV.B.

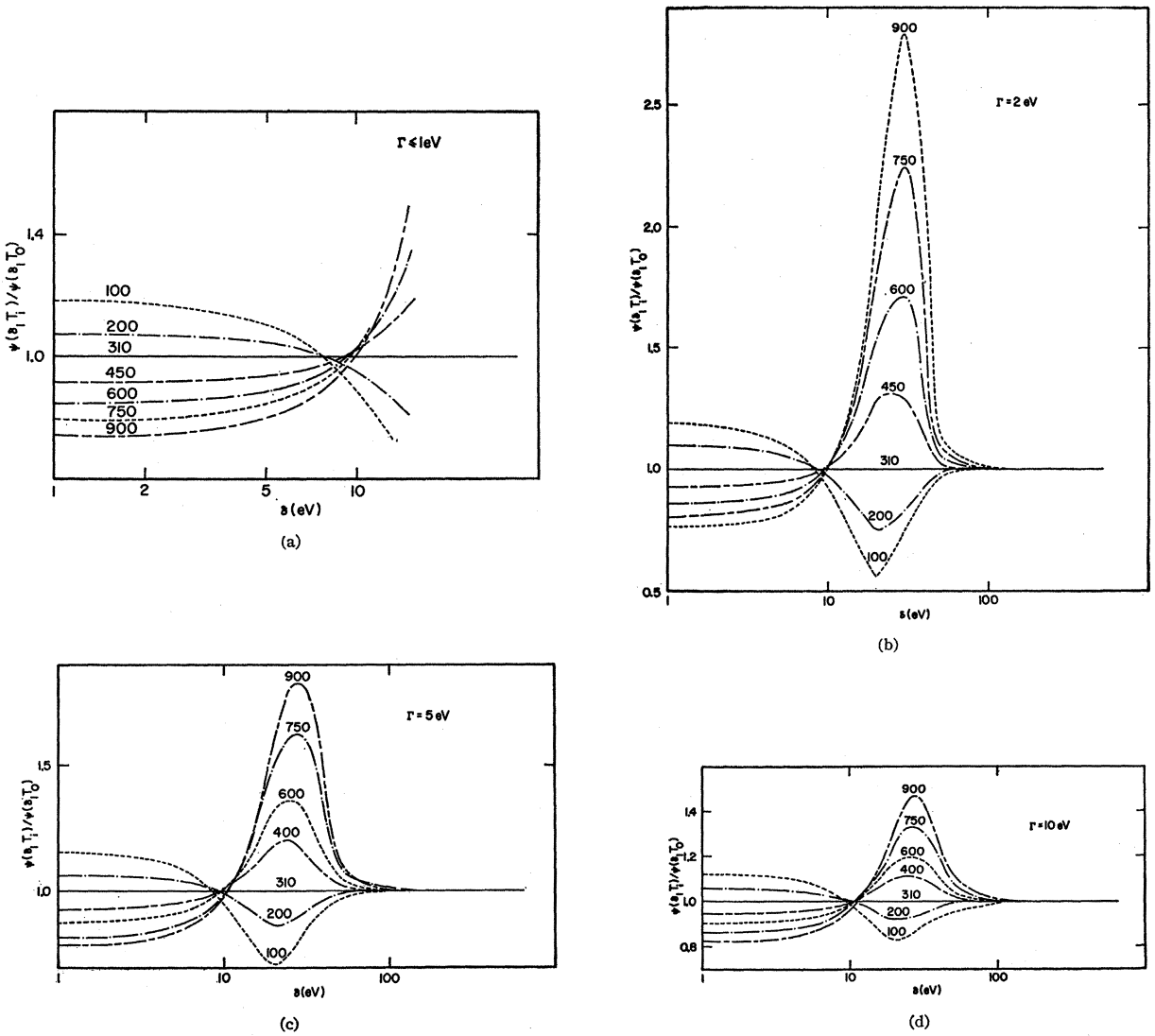

FIG. 6. Expected variation in counting rate of resonant scattered gamma rays as a function of scatterer temperature, for different values of δ and Γ. Calculated for the 8.499-MeV resonance in copper. The figures on the curves give the effective temperature in °K. The ratio of counting rates is given relative to 310°K. (a) $\Gamma \leq 1$ eV; (b) $\Gamma=2$ eV; (c) $\Gamma=5$ eV; (d) $\Gamma=10$ eV.

The theoretical value of R is evaluated in Appendix A, for the case $\Gamma \ll \Delta_i$.

To a good approximation, R is given by

$$R=\Gamma_0 \pi^{3/2} \lambda^2 g \frac{ND}{\Delta_i}\left(\frac{1+f}{2+f}\right)^{1/2} \times \exp\left[-\left(\frac{f\delta^2}{(1+f)(2+f)\Delta_e^2}\right)\right], \quad (23)$$

where D is the absorber thickness, and $f=(\Delta_i/\Delta_e)^2$, the square of the ratio of Doppler widths of target and source nuclei. It can be seen that R depends only on Γ_0 and δ, and is independent of Γ the total level width.

4. EXPERIMENTAL RESULTS

A. Measurements of the Effective Cross Sections

The effective cross sections were evaluated using the appropriate form of Eq. (8).

In many cases it was not possible to measure directly the counting rate C_0 of the photopeak corresponding to the resonance energy. This was usually due to prominent capture gamma rays of higher or adjacent energies obscuring the required photopeak in the direct spectrum. C_0 was therefore estimated indirectly using the measured response curve of the crystal and the relative intensities of capture gamma rays reported in the literature.[6] As there are considerable differences in the intensities given by the various groups, in each case

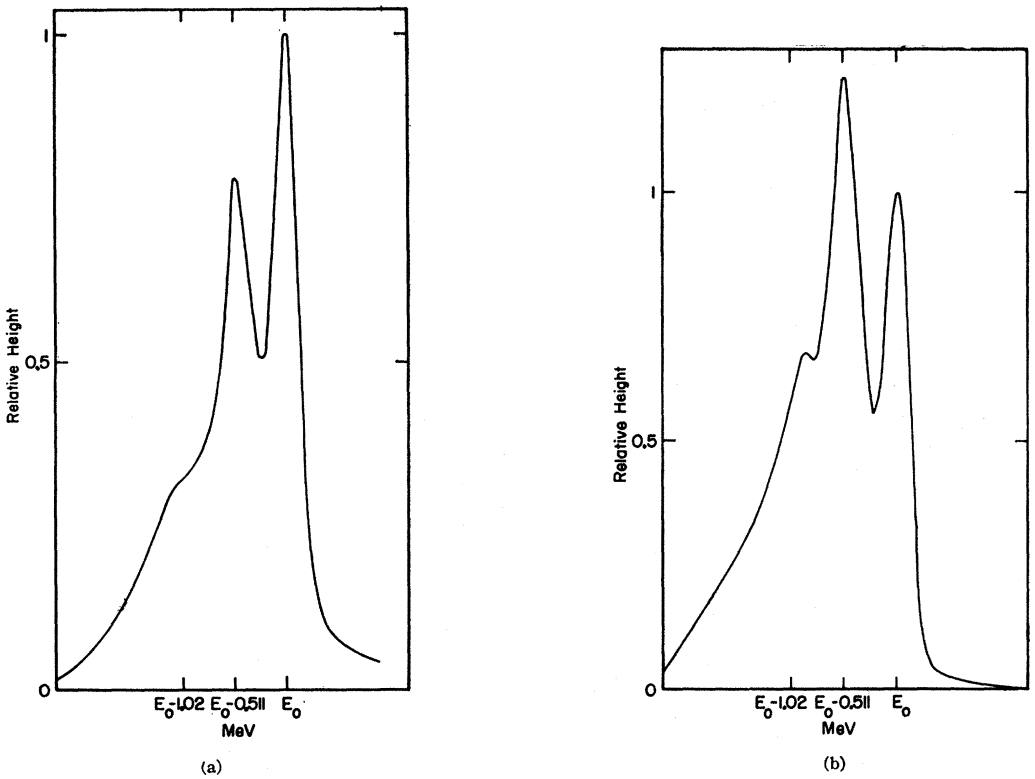

FIG. 7. (a) Response curve of the 5-in.-diam, 5-in.-thick NaI(Tl) crystal for a 7.639-MeV collimated direct beam of 52-mm diameter. (b) Response curve of the 5-in.-diam, 5-in.-thick NaI(Tl) crystal for a 7.28-MeV beam scattered from lead, with a target to detector distance of 17 cm.

the set used was that which gave the best fit to the recorded spectrum.

The crystal response curve for the collimated "direct" geometry was measured using simple capture spectra having one dominant line, e.g., the 7.639-MeV line of $Fe^{56}(n\gamma)$ and the 7.724 line of $Al^{27}(n\gamma)$. These response curves were corrected by subtracting the estimated contribution due to weaker lines, using the tabulated relative intensities, and the resulting curve for Fe^{56} is shown in Fig. 7(a). The response curve for the scattered line of 7.28 MeV [$Fe^{56}(n\gamma)$], on Pb, is shown in Fig. 7(b). Using these two curves the ratio of the photofractions for the direct and scattered geometries has been evaluated, giving $\eta_0/\eta_{sc}=1.30\pm0.05$. This can be expected to remain fairly constant, to within the stated error, over the energy range of 7–9 MeV.

The calculated values of $\langle\sigma_{\gamma\gamma}\rangle$ are shown in Table III, for the 20 resonance events detected so far. Those values suspected of possessing a large systematic error, due to large discrepancies in the reported relative intensities, are marked with an asterisk. Some of the figures differ with earlier reported values, owing to improved experimental data and more precise calculations.

Several of the resonances were studied in further detail by varying the scatterer temperature, or by carrying out a self-absorption experiment. These are discussed below.

B. The 7.639-MeV Resonance in Nickel

The effective cross section $\langle\sigma_{\gamma\gamma}\rangle$ was found to be 10.5 mb for this resonance. There was a pronounced temperature effect in the range 77 to 900°K, as shown in Table IV.

Analysis of the observed temperature variation gave a solution for δ the separation between the gamma line and resonance energy of $\delta=12\pm1$ eV.

The evaluation of Γ, the level width, requires a knowledge of the nuclear spin factor g, and hence the spins of the excited and ground states. As all the natural nickel isotopes are even-even nuclei—except for the 1.25% abundant Ni^{61}—the spin of the ground state can be taken to be 0. An angular correlation experiment was carried out to measure the spin of the excited state by measuring the ratio of photons scattered at 135° and at 90°. The nickel scatterer was set with its normal at 67.5° to the beam direction, so as to equalize the electronic absorption at the above two angles. The measured ratio was found to be 1.7 ± 0.1. Using the tables of Fraunfelder[17] for a ground-state spin $I_g=0$,

[17] H. Frauenfelder, in *Beta and Gamma-Ray Spectroscopy*, edited by K. Siegbahn (North-Holland Publishing Company, Amsterdam, 1955), p. 910.

TABLE III. Effective cross sections.

γ source	Energy (MeV)	Scatterer Element	Protons	Neutrons	$\langle\sigma_{\gamma\gamma}\rangle$ (mb)	Notes
Hg	5.44	Hg	80	116, 118, 119, 120, 121, 122, 124	128	
Cl	6.12	Pr^{141}	59	*82*	103	a
V	6.508	Sn	*50*	62, 64–70, 72	14	
Co	6.690	Pr^{141}	59	*82*	2.7	a
Co	6.867	Nd	60	82, 83, 84, 85, 86, 88	22	
Al	6.98	Pb^{208}	*82*	*126*	2900	b
Cl	6.98	Pb	*82*	124, 125, *126*	346	a
Ti	6.996	Bi^{209}	83	*126*	1560	b
Cu	7.01	Sn	*50*	62, 64–70, 72	1000	b
Ti	7.149	Pb^{208}	*82*	*126*	1000	b
Co	7.201	Pb^{208}	*82*	*126*	25	
Mn	7.261	Pb^{208}	*82*	*126*	25	a
Fe	7.285	Pb^{208}	*82*	*126*	4100	a
V	7.305	Pb^{208}	*82*	*126*	12.5	
Hg	7.32	Pb	*82*	124, 125, *126*	5500	c
Fe	7.639	Ni	*28*	30, 32, 34, 36	10.5	d
Fe	7.639	Pr^{141}	59	*82*	10	d
Cr	8.499	Cu	29	34, 36	24.4	
Cr	8.881	Pr^{141}	59	*82*	9.3	
Ni	8.997	Sm	62	*82*, 85–88, 90, 92	2.8	

[a] A large error could be introduced in the cross-section values because of large differences in line intensities quoted by Bartholomew and Higgs and by Groshev *et al.* (Ref. 6).
[b] Because of the low counting rate, thick scatterers were used, which will introduce a systematic error in estimating $\langle\sigma_{\gamma\gamma}\rangle$ for resonances having a high nuclear cross section.
[c] The cross section was evaluated assuming the gamma intensity to be 0.02 photons per 100 captured neutrons (see text).
[d] Reference 6 gives the 7.639 line of iron capture gamma rays as a single line. However, a recent paper by Fiebiger, Kand, and Segel [Phys. Rev. **125**, 2031 (1962)] reports two different lines of equal intensities having energies of 7.647 and 7.633 MeV. The present experiment cannot resolve an energy difference of 14 keV, therefore, there is no possibility of deciding which line is responsible for the scattering.

the ratio of intensities at these two angles is given by

$$W(135°)/W(90°)=\tfrac{3}{2} \text{ for dipole transition}$$
$$=\tfrac{1}{2} \text{ for quadrupole transition.}$$

This clearly shows the dipole nature of the transition and the excited state thus has a spin of 1. In addition, it can be deduced that the resonant condition is not caused by the Ni^{61} isotope, as its ground-state spin is $\frac{3}{2}^-$. It is not possible from these results to decide which of the four even-even nickel isotopes is responsible for the resonance. The level width can now be calculated from Eqs. (9) and (10). If we assume $\Gamma_0/\Gamma\sim 1$, then Γ_0 can be expressed as $\Gamma_0=(3.28_{-0.50}{}^{+0.70})/a$ meV, where a is the fractional isotopic abundance (0.68 for Ni^{58}, 0.26 for Ni^{60}, 0.037 for Ni^{62}, and 0.011 for Ni^{64}). Identification of the particular isotope would require several tens of grams of enriched nickel isotopes.

C. The 8.499-MeV Resonance in Copper

The effective cross section $\langle\sigma_{\gamma\gamma}\rangle$ was found to be 24 mb. This corresponds to a cross section per scattering nucleus of 35 mb if the 69% Cu^{63} isotope is responsible for the resonance and of 80 mb if the resonant level is in the 31% abundant Cu^{65}. The scattered intensity remained constant to within $\pm 1\%$ for scatterer temperatures in the range 77 and 900°K. This permits fixing lower limits to the separation δ and the level width, as the temperature variation of the scattered photons becomes progressively smaller at larger values of δ, many times the Doppler width. If the upper limit of the temperature variation is taken as 2% over the above temperature range, then possible solutions would be $\delta=120$ eV, $\Gamma=7.5$ eV for Cu^{63}, and $\delta=120$ eV, $\Gamma=10.5$ eV for Cu^{65}. Larger values of δ would give a still smaller temperature variation, but would require even larger level widths to explain the observed cross section.

The presence of such a broad level in copper can be compared with the results of the earlier poor resolution experiments,[1] where the energy resolution was about 0.5 MeV. The average elastic scattering cross section was found to be 0.5 mb in the energy region of 8.5 MeV. This integral cross section could be produced by a single level of 7-eV width in Cu^{63} or a level of 15-eV width in Cu^{65}. The present results are therefore consistent with a single broad level causing most of the nuclear elastic scattering in this energy region.

There is another possible interpretation of the small temperature variation for the copper resonance. Figure

TABLE IV. Temperature effect for 7.639 MeV in nickel.

Temperature, °K	77	300	600	900
Effective temperature, °K	150	320	610	900
Relative intensity	0.84±0.02	1	1.25±0.03	1.38±0.03

6 shows the temperature variation as a function of the separation energy δ. There is a minimum for $\delta=9$ eV, corresponding to a predicted temperature variation of 3% in the range 77–900°K. This value is just consistent with the experimental values, the discrepancy being about twice the probable error. For this value of δ, the corresponding natural width of the resonant level can be determined, using Eqs. (9) and (10).

$$\Gamma_0=26 \text{ meV for } Cu^{63},$$

$$\Gamma_0=57 \text{ meV for } Cu^{65}.$$

It is assumed that the nuclear g factor is unity for the above values. Other values consistent with a dipole transition are $g=\frac{1}{2}$, $g=\frac{3}{2}$. The corresponding natural widths can be obtained by dividing the $g=1$ results by the required g factor.

The copper results thus permit two quite diverse interpretations. It is proposed to solve this difficulty by varying the separation energy δ using the technique discussed in Sec. II G. If δ is actually 9 eV, then a variation of a few eV will produce a large variation in the intensity of the scattered photons.

D. The 7.285-MeV Resonance in Lead

By using scatterers of different isotopic abundance this resonance has been identified as due to Pb^{208}, the effective cross section per Pb^{208} nucleus being 4.1 b. The angular distribution has been measured previously,[7] thus, permitting evaluation of the spin factor g. In addition, analysis of the temperature variation between 77 and 400°K permitted an estimation of $\delta=8.5\pm0.5$ eV.

As the nuclear cross section in this case is comparable with the electronic cross section it was possible to carry out a self-absorption experiment. For a scatterer thickness of 3.25 g/cm^2 and absorber thickness 15.84 g/cm^2, the self-absorption ratio was found to be $R=0.30\pm0.01$. Using these values in Eq. (A11) the level width Γ_0 was found to equal 0.8 ± 0.03 eV.

Using the above values of δ and Γ_0 in Eq. (19), $\langle\sigma_{\gamma\gamma}\rangle$ can be evaluated, giving $\langle\sigma_{\gamma\gamma}\rangle=(4, 4\pm0.15)(\Gamma_0/\Gamma)^2$ b, in excellent agreement with the experimental value. This suggests that $\Gamma_0/\Gamma\sim1$ for this resonance level.

In deriving Eq. (A11) the shape of the resonance level was assumed to have the pure Doppler form, to permit a simple evaluation of the integrals. Generally this approximation is not valid for $\Gamma\sim\Delta$, which applies in this case since $\Delta=3.7$ eV. However, for the particular case of $\delta\sim10$ eV, numerical results obtained using the Doppler approximation almost coincide with those using the general expressions for $\sigma(E)$.[15]

E. The 7.3-MeV Resonance on Lead (Produced by Capture Gamma Rays from Mercury)

As can be seen from Fig. 5 there is a clear resonance at about 7.3 MeV. However no line of this energy has been reported in the capture gamma rays produced by thermal neutron capture in mercury.[6] Other possible causes of this resonance were therefore considered. Neutrons absorbed in the lead target could produce capture gamma rays of 7.38 MeV, however, the addition of neutron absorbing material in the beam showed no appreciable attenuation in the intensity of scattered gammas. Another possible explanation is the (γn) interaction in Pb^{207} produced by photons above 6.73 MeV inside the lead scatterer, the neutrons then interacting to give capture gamma rays. To test this possibility equal mass lead and bismuth absorbers were placed alternately before the crystal—and gave exactly the same attenuation. This shows the absence of any additional neutrons produced in the scatterer.

We believe that this resonance is caused by a hitherto undetected line of 7.3-MeV energy in the capture gamma-ray spectrum of mercury. Studies of neutron resonance capture in Hg^{201} shows a 7.32-MeV transition for the 43-, 71-, and 210-eV resonances.[18] Owing to the large 2500-b cross section in Hg^{199}, the thermal neutron capture cross section in Hg^{201} has not been measured directly but has been estimated as less than 60 b.[6] If this cross section is a few barns then one could expect the 7.32-MeV transition to occur with an intensity of the order of 0.01–0.02 photons/100 neutrons captured in natural mercury. Such an intensity would not have been detected in the thermal neutron capture gamma-ray measurements.[6] Taking a value of 0.02 photon/100 neutrons captured, the effective cross section is estimated as 5.5 b. This value has been confirmed by a self-absorption experiment. A temperature variation experiment is being carried out and it is intended to make an estimate of the actual intensity of 7.32-MeV gammas in the mercury spectrum.

V. DISCUSSION

An examination of Tables II and III shows that the occurrence of these resonance events is a selective phenomenon, predominantly at or near closed-shell nuclei. Of the 20 resonances reported here all are consistent with the resonant nucleus being at most two nucleons from a closed shell. [A further 12 resonances have been found in an additional survey using some thirty additional scatterers. The events occur in lanthanum (3), cadmium (3), molybdenum (2), tellurium (1), cerium (1), and thallium (2), all close to closed shells of nucleons.[18a]] Of particular significance is the large number of resonances found in Pb^{208}, a doubly "magic" nucleus, which shows that a high probability for nuclear resonant scattering is connected with closed shells of nucleons. This magic number dependence has already been pointed out by the present

[18] R. T. Carpenter and L. M. Bollinger, Nucl. Phys. **21**, 66 (1960).

[18a] *Note added in proof.* Up to now a total of more than 60 clear examples of resonance effects have been observed.

authors[19] and independently by Axel.[20] A similar effect was reported by Reibel and Mann.[2] This type of experiment is selective for those levels having large values of the branching ratio and transition probabilities to the ground state, which is a feature of closed-shell nuclei. In addition, resonance scattering should be more predominant in regions having large values of the strength function.

The discovery of such large numbers of resonances is in apparent contradiction to earlier work. Only one resonance was reported by Young and Donahue,[7,21] the 7.285 resonance using iron capture gamma rays on lead. They found no evidence for resonance scattering using titanium capture gammas on bismuth and lead, and manganese capture gammas on lead, which were found in the present work. This discrepancy is probably caused by the differences in experimental technique between the two experiments. Young and Donahue used a radial beam tube, looking directly at the reactor core. Hence, despite considerable shielding, a large flux of fast neutrons remained in the beam—about 200/cm^2·sec·MeV—which undoubtedly contributed to the background in the detector. In the present experiment the fast neutron flux scattered into the detector from the thermal column was less than 5 neutrons/cm^2·sec. The considerable shielding around the detector and scatterer also contributed to a reduction in over-all background to some 5% of that encountered in the earlier experiment.

The detection of a particular resonance level requires that the scattered gamma rays be detectable above the nonresonant background. The minimum detectable effective cross section $\langle\sigma_{\gamma\gamma}\rangle_{\min}$ varies considerably, by up to three orders of magnitude, depending on the intensity of the gamma line responsible for the resonance, and the background at that energy region. The intensity of the gamma lines is given by the relative abundance for the particular source, and the source geometry and capture cross section for thermal neutrons. This can vary by several orders of magnitude. The variation in background is much less than this, being of the order of a factor of 10 in the region 7–9 MeV, the background rising steeply at low energies. It is also somewhat larger for scattering targets of higher Z and mass.

The resonances found for lead could be divided into two energy groups—6.8 to 7.2 MeV and 7.2 to 7.4 MeV—corresponding to the concentrations in strength function recently reported around 7.03 and 7.29 MeV by Axel *et al.*[5] The results in the present work show that the 7.285-MeV resonance is caused by a level of 0.8-eV width and peak separation δ of 8.5 eV. This can be compared with Doppler-limit approximations of 0.6±0.2 eV for the level width and $\delta=10\pm2$ eV obtained by Young and Donahue.[21] This is in disagreement with Axel *et al.*[5] who suggest a single broad level of 40-eV width as responsible for the resonant scattering around 7.29 MeV.

All the scattered spectra of the lead resonances show a shape fully consistent with a single-photon energy with no sign of any low-energy contribution, which could be expected to be present if there was an inelastic scattering component. In the one case where self-absorption was measured, the branching ratio was found to be within 5% of unity. This could be expected owing to the lack of any levels in Pb^{208} below 2.6 MeV. Even for those levels immediately above this region, the spin assignment would not permit an electric dipole transition from a 1^- state. All the above resonances in Pb^{208} are being studied systematically using temperature variation and, where possible, self-absorption techniques so as to obtain the widths of the various levels responsible for the resonant scattering. This will be reported elsewhere.

ACKNOWLEDGMENTS

The authors wish to thank I. Bala, H. Herman, and A. Ziv of the technical services department for their assistance in design and construction of the experimental equipment. We are particularly indebted to the reactor operating staff of the I.R.R.1 research reactor. We are also grateful to Dr. P. Axel, Dr. D. J. Donahue, and Dr. C. S. Young for making available their results before publication.

APPENDIX A: EVALUATION OF THE RATIO R FOR THE SELF-ABSORPTION EXPERIMENT

The partial level width for the ground-state transition of the resonance level can be determined by inserting a thin target of the scattering material in the incident beam before the main scattering target. This is only possible where $\sigma_n\sim\sigma_e$. Hence, Eq. (3b) applies for the intensity reaching the detector. Without the absorber,

$$I_{sc}=A\int_0^\infty \sigma_{\gamma\gamma}(E)F(E)dE-B\int_0^\infty \sigma_{\gamma\gamma}{}^2F(E)dE, \quad \text{(A1)}$$

where

$$A=\frac{\Delta\Omega x_0 N}{11.2}\left[1-\frac{Nx_0}{2}(1+\sqrt{2})\sigma_e\right], \quad \text{(A2)}$$

$$B=\frac{\Delta\Omega}{11.2}\frac{N^2x_0{}^2}{\sqrt{2}}\frac{\Gamma}{\Gamma_0}, \quad \text{(A3)}$$

where the relation $\sigma_n=(\Gamma/\Gamma_0)\sigma_{\gamma\gamma}$ has been used in (3b).

[19] G. Ben-David, B. Huebschmann, and I. Pelah, Israel Atomics-822, p. 36 (unpublished).
[20] P. Axel, Phys. Letters 4, 320 (1963).
[21] C. S. Young and D. J. Donahue, Phys. Rev. 133, 1724 (1963).

Consider a resonant absorber of thickness D in the incident beam. Equation (A1) is now modified

$$I_{sc}(\text{res})=A\int_0^\infty e^{-(\sigma_n+\sigma_e)ND}\sigma_{\gamma\gamma}(E)F(E)dE - B\int_0^\infty e^{-(\sigma_n+\sigma_e)ND}\sigma_{\gamma\gamma}{}^2F(E)dE. \quad \text{(A4)}$$

A "nonresonant" absorber is now chosen of an element adjacent to the resonant absorber, and having the same thickness for electronic absorption $\sigma_e ND$, but no nuclear resonance absorption. For this case, we can write

$$I_{sc}(\text{nonres})=A\int_0^\infty e^{-\sigma_e ND}\sigma_{\gamma\gamma}(E)F(E)dE - B\int_0^\infty e^{-\sigma_e ND}\sigma_{\gamma\gamma}{}^2F(E)dE. \quad \text{(A5)}$$

Over the energy interval of interest the electronic cross section is insensitive to energy changes, and $e^{-\sigma_e ND}$, can be taken outside the integrals. Defining the ratio

$$R=\frac{I_{sc}(\text{nonres})-I_{sc}(\text{res})}{I_{sc}(\text{nonres})},$$

we find

$$R=\left[A\int_0^\infty(1-e^{-\sigma_n ND})\sigma_{\gamma\gamma}F(E)dE-B\int_0^\infty(1-e^{-\sigma_n ND})\sigma_{\gamma\gamma}{}^2F(E)dE\right]\Big/ \left[A\int_0^\infty\sigma_{\gamma\gamma}F(E)dE-B\int_0^\infty\sigma_{\gamma\gamma}{}^2F(E)dE\right]. \quad \text{(A6)}$$

As a thin target was chosen (with respect to the nuclear absorption) we can expand the exponential term, obtaining $1-e^{-\sigma_n ND}=\sigma_n ND-\frac{1}{2}(\sigma_n ND)^2$, neglecting terms higher than the second order. Introducing this into (A6) we obtain

$$R=ND-\frac{\Gamma}{\Gamma_0}\frac{A\langle\sigma_{\gamma\gamma}{}^2\rangle-[\frac{1}{2}A(\Gamma/\Gamma_0)ND+B]\langle\sigma_{\gamma\gamma}{}^3\rangle+\frac{1}{2}B(\Gamma/\Gamma_0)\langle\sigma_{\gamma\gamma}{}^4\rangle ND}{A\langle\sigma_{\gamma\gamma}\rangle-B\langle\sigma_{\gamma\gamma}{}^2\rangle}, \quad \text{(A7)}$$

where

$$\langle\sigma_{\gamma\gamma}{}^j\rangle=\int_0^\infty\sigma_{\gamma\gamma}{}^jF(E)dE\Big/\int F(E)dE. \quad \text{(A8)}$$

In general, the evaluation of $\langle\sigma_{\gamma\gamma}{}^j\rangle$ is difficult, involving an integration of powers of the function Ψ defined by Eq. (11).

However, for the extreme case $\Gamma\ll\Delta_e$, the expression for $\sigma_{\gamma\gamma}$ is well approximated[12] by

$$\sigma_{\gamma\gamma}(E)=\sigma_{\max}{}^0\pi^{1/2}\frac{\Gamma}{2\Delta_i}\exp\left\{-\left[\frac{(E-E_R)^2}{\Delta_i{}^2}\right]\right\}. \quad \text{(A9)}$$

The integrals (A8) can then be evaluated yielding

$$\langle\sigma_{\gamma\gamma}{}^j\rangle=\left(\sigma_{\max}{}^0\frac{\pi^{1/2}}{2}\frac{\Gamma}{\Delta_i}\right)^j\left(\frac{f}{j+f}\right)^{1/2}\exp\left[-\frac{j\delta^2}{(j+f)\Delta_e{}^2}\right], \quad \text{(A10)}$$

where $f=(\Delta_i/\Delta_e)^2$ the ratio of the square of the Doppler widths of target and source nuclei and δ is the energy separation between the photon and resonance level.

Inserting the values of $\langle\sigma_{\gamma\gamma}{}^i\rangle$ from (A10) into (A7) and substituting for $\sigma_{\max}{}^0$ from Eq. (10), we obtain

$$R=\Gamma_0 K\times\frac{\left(\frac{1}{2+f}\right)^{1/2}\exp\left[-\frac{2\delta^2}{(2+f)\Delta_e{}^2}\right]-\left(\frac{1}{2}+\frac{x_0}{D}\frac{1}{\sqrt{2}T}\right)K\Gamma_0\left(\frac{1}{3+f}\right)^{1/2}\exp\left(-\frac{\delta^2}{\Delta_e{}^2}\frac{3}{3+f}\right)+\frac{x_0}{2\sqrt{2}TD}K^2\Gamma_0{}^2\left(\frac{1}{4+f}\right)^{1/2}\exp\left(-\frac{\delta^2}{\Delta_e{}^2}\frac{4}{4+f}\right)}{\left(\frac{1}{1+f}\right)^{1/2}\exp\left(-\frac{\delta^2}{\Delta_e{}^2}\frac{1}{1+f}\right)-\frac{x_0}{\sqrt{2}DT}K\Gamma_0\left(\frac{1}{2+f}\right)^{1/2}\exp\left(-\frac{\delta^2}{\Delta_e{}^2}\frac{2}{2+f}\right)}, \quad \text{(A11)}$$

where $K=ND\pi^{3/2}(\lambda^2/\Delta_i)g$ and $T=1-NX_0(\frac{1}{2}+\frac{1}{2}\sqrt{2})\sigma_e$.

If the terms including $K\Gamma_0$ in the numerator and denominator are neglected, R is approximated by

$$R=\Gamma_0 N D\pi^{3/2}\frac{\lambda^2}{\Delta_i}g\left(\frac{1+f}{2+f}\right)^{1/2}\exp\left[-\frac{f\delta^2}{(2+f)(1+f)\Delta_e^2}\right]. \quad \text{(A12)}$$

The solution of (A12) gives a first approximation to Γ_0, which can be solved from Eq. (A11) using an iterative technique.

PHYSICAL REVIEW VOLUME 133, NUMBER 3B 10 FEBRUARY 1964

Reactions Induced in Fe^{54} with 21–63 MeV Li^6 Ions*

MARSHALL BLANN, FRANK M. LANZAFAME, AND R. AMELIA PISCITELLI
Department of Chemistry, University of Rochester, Rochester, New York
(Received 25 September 1963)

Excitation functions have been measured for the production of Ni^{56}, Ni^{57}, Co^{55}, Co^{56}, Co^{57}, Co^{58}, Fe^{52}, Fe^{55}, and Mn^{54} from Fe^{54} bombarded with Li^6 ions of 21–63-MeV kinetic energy. The targets were enriched to 95% Fe^{54}. Excitation functions for the production of Ni^{57}, Co^{55}, Co^{56}, Co^{57}, Fe^{55}, and Mn^{54} resulting from Li^6 bombardment of Fe^{54} and deuteron bombardment of Ni^{58} are compared. Of these, excitation functions for the production of Ni^{57}, Co^{57}, and Mn^{54} are mutually consistent with decay of a Cu^{60} compound nucleus. Excitation functions for production of Co^{55} and Fe^{55} with the two projectiles appear to proceed by different mechanisms. The Co^{56} excitation functions in the two target-projectile systems are not directly comparable, since the probable reactions producing Co^{56} are $Ni^{58}(d,\alpha)Co^{56}$ and $Fe^{54}(Li^6,2p2n)Co^{56}$. All excitation functions studied in the $Fe^{54}+Li^6$ system show the competitive behavior of compound-nucleus reactions with the exception of the high-energy tail of the Co^{58} excitation function (apparently due to 5% Fe^{56} impurity in the targets) and the low-energy portions of the Co^{55} and Fe^{55} excitation functions. The very low yields observed for the production of Ni^{56} and Ni^{57} are attributed to the effect of the 28-nucleon shells on nuclear level densities. The sum of measured cross sections from $Fe^{54}+Li^6$ reactions is compared with calculated optical-model nonelastic cross sections.

I. INTRODUCTION

THE present work describes experimental results of measurements of excitation functions resulting from the Li^6 bombardment of Fe^{54}. The investigation was undertaken as part of a general study of the compound-nucleus reaction mechanism, with particular interest in the applicability of statistical theory to the decay of the compound nucleus. Reactions at intermediate energies are, in general, mixtures of direct interaction and compound-nucleus processes. It is meaningless to compare predictions of the statistical theory with experimental results corresponding to direct interactions. For this reason one must first have at least qualitative evidence that a given set of reactions proceeds predominantly by the compound-nucleus mechanism before applying statistical mechanics for a theoretical prediction of decay products. To provide such qualitative evidence was the general motivation for undertaking this work.

The system selected for this study ($Fe^{54}+Li^6$) was chosen for several reasons. First, the compound nucleus formed (assuming one is formed) is Cu^{60}, which is the same compound nucleus formed with deuterons incident on Ni^{58}. The yields of reaction products formed in the $Ni^{58}+d$ system were shown to be fairly consistent with formation from the decay of a compound nucleus at statistical equilibrium.[1] The highest excitation energy produced with deuterons on Ni^{58} corresponds roughly to the lowest excitation energy produced with Li^6 ions on Fe^{54} in this work. Both systems have approximately the same average angular momentum in the overlapping region as well. Hence, if the relative yields of the decay products are the same for both systems in this region, there is additional evidence for considering both reactions as proceeding through a compound-nucleus mechanism. The $Fe^{54}+Li^6$ system may then be studied at higher excitations (and with higher angular momentum) than the $Ni^{58}+d$ system, since Li^6 ions of up to 63 MeV are available. One may then see if these reactions appear to be proceeding by the compound-nucleus mechanism to the highest excitations measured, and if so, determine whether or not the results are consistent with decay of a compound nucleus at statistical equilibrium.

Additional interest in study of reactions in this region lies in the relatively low yields of Ni^{56} and Ni^{57} with

* This work supported by the U. S. Atomic Energy Commission.

[1] M. Blann and G. Merkel, Phys. Rev. **131**, 764 (1963).